ISSN No:-2456-2165 https://doi.org/10.38124/ijisrt/25jul1701

Temperature-Energy Relationships and Spatial Distribution Analysis for Nano-Enhanced Phase Change Materials Via Thermal Energy Storage

Florence Awuor Misawo[1]; Fredrick O. Nyamwala[2]; Onyango Thomas T. Mboya[3]

[1;2]Department of Mathematics School of Biological & Physical Science Moi University, Eldoret Kenya
[3]Department of Mathematics and Statistics, Technical University of Kenya

Publication Date: 2025/08/02

Abstract: This study investigates the thermal performance of nano-enhanced phase change materials (NEPCMs) for thermal energy storage (TES) applications, focusing on their energy behavior during phase transitions. The primary objective was to model and compare the heat storage capabilities of NEPCMs, specifically involving aluminum oxide (Al_2O_3) nanoparticles, and pure water, using a finite control volume approach to simulate the governing energy equations. Thermophysical properties such as density, specific heat capacity, thermal conductivity, and volumetric expansion were defined for both base PCMs and nanoparticles to derive effective NEPCM properties. Using MATLAB, discretized equations were implemented to analyze spatial and temperature-dependent energy variations across a two-dimensional domain. Key findings demonstrate that NEPCMs exhibit sharper and more localized energy peaks, attributed to latent heat effects and enhanced thermal conductivity. In contrast, water exhibited broader, smoother energy profiles due to its high specific heat capacity and lack of phase transitions in the studied temperature range. Visualization through 3D surface plots and scatter plots confirmed that NEPCMs enable faster charging/discharging and improved thermal regulation, making them suitable for dynamic TES applications such as solar energy harvesting, electronic cooling, and waste heat recovery. This research underscores the importance of integrating nanoparticles into PCMs to optimize thermal responsiveness and efficiency, and recommends further work in optimizing nanoparticle volume fractions and incorporating transient convection models.

Keywords: *Nano-Enhanced Phase Change Materials; Phase Change Process; Energy Storage; Finite Volume Method.*

How to Cite: Florence Awuor Misawo; Fredrick O. Nyamwala; Onyango Thomas T. Mboya (2025) Temperature-Energy Relationships and Spatial Distribution Analysis for Nano-Enhanced Phase Change Materials Via Thermal Energy Storage. *International Journal of Innovative Science and Research Technology*, 10(7), 2705-2722. https://doi.org/10.38124/ijisrt/25jul1701

I. INTRODUCTION

➢ *Background Information*

The quest for clean, sustainable sources of energy is becoming more popular with the concerns over global warming [32]. Scientists have established that carbon dioxide emissions, from the use of fossil fuels contribute to the greenhouse effect. Solar energy is unlimited and harnessing it for heating and electricity is pollution free. Development of solar energy equipment among them being solar cookers can help our environment by decreasing emissions [17]. In addition, solar energy is renewable and readily available. One major drawback in harnessing is its availability only during sunshine, presenting major challenge to its use in the dark. Solar radiation is intermittent, irregular in nature and its storage is essential in order to optimize its usage.

Collection of solar energy is done by the use of a parabolic trough as shown in Figure 1. This is then directed to a focal point where the receiver stands to absorb it. Vapor is generated in the heat absorber at the focal point of the parabolic concentrator and condensed in a coiled tube, which is casted into an aluminum plate [22]. Heat transfer is by a thermo-syphon principle, with water as the working fluid at about 35-bar pressure. The heating plate has heat-conducting rods extended into a phase change storage system (Nitrate mixture). Thermal energy is stored in the form of Latent heat which the research is based on using Partial Differential Equations (PDEs).

ISSN No:-2456-2165 https://doi.org/10.38124/ijisrt/25jul1701

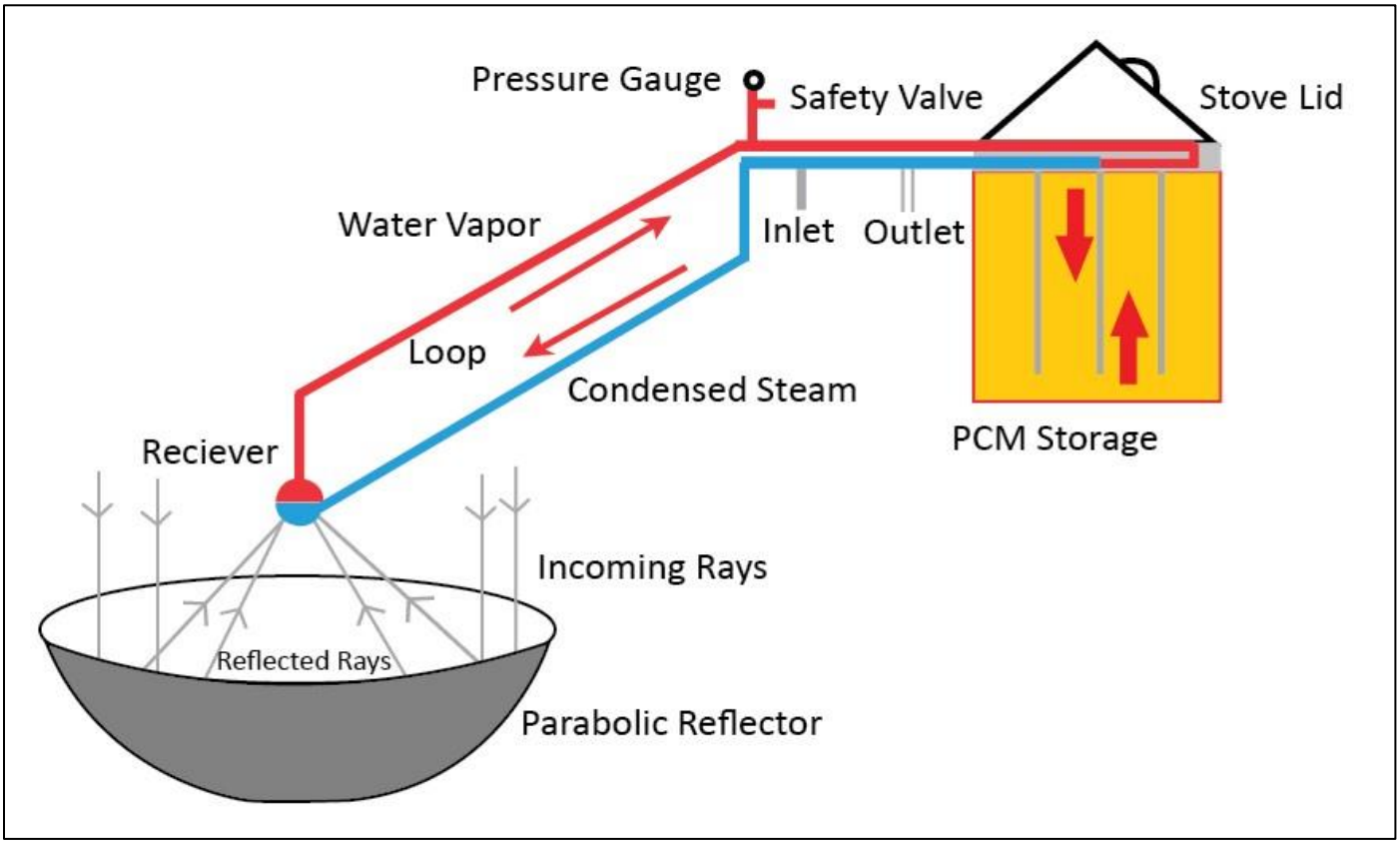

Fig 1 Illustration on Collection and Storage of Solar Energy

The basic mechanisms of heat transfer are conduction, convection and radiation [36]. Conduction is the transfer of energy from the more energetic particles of a substance to the adjacent less energetic ones as a result of interaction between particles. Convection is the mode of heat transfer between a solid surface and adjacent liquid or gas which is in motion and it involves the combined effects of conduction and fluid motion. According to [34], transfer of solar energy by radiation is where the energy emitted by matter is in the form of electromagnetic waves (or photons) as a result of the changes of the electronics configuration of the atoms or molecules.

There are three forms of heat energy storage namely sensible heat, latent heat and thermo-chemical or combination of these [12]. Sensible heat storage (SHS) is a criterion for storing thermal energy by raising the temperature of a solid or liquid [6]. SHS system utilizes heat capacity and change in temperature of the material during the process of charging and discharging. The amount of heat stored depends on the specific heat of the medium, the temperature change and the amount of storage material.

Total enthalpy H is computed as the sum of the sensible enthalpy, h and the latent heat ΔH [44]

$$H = h + \Delta H \quad (1)$$

Where

$$h = h_{ref} + \int_{T_{ref}}^{T} C_p dT \quad (2)$$

In quation (2) h_{ref} and T_{ref} denote the reference enthalpy and reference temperature respectively, C_p represents the specific heat. $\Delta H = f_1 L$, where L is the latent heat of PCM and f_1 is the liquid fraction.

Latent heat storage (LHS) is based on the heat absorption or release when a storage material undergoes a phase change from solid to liquid or liquid to gas or vice versa at constant temperature [25]. Latent heat is an attractive way to store solar thermal energy as it provides high storage density where a lot of energy can be stored in a very small volume. The phase change process occurs at nearly constant temperature, which is a fundamental aspect for efficient operation of most thermal systems [31]. An advantage of LHS relative to SHS is that the temperature of the phase change material (PCM) may be closer to the environment temperature thereby minimizing heat loss or gain. In addition, the driving temperature of a LHS system can remain nearly constant between a heat transfer surface and the PCM during both charging and discharging which may vary greatly during operation for the SHS system. These properties along with the higher energy density make LHS an attractive form of thermal storage, particularly for portable appliances which is not practical for SHS systems [35].

The principle of thermochemical heat storage uses the energy from an exothermic reaction for the application, and charge the storage by running the corresponding endothermic reaction [18]. The storage potential of thermochemical energy is very important and research on improvements are intensively conducted both for large size seasonal and small size modules. PCM is a substance having a high heat of fusion which, on melting and solidifying at a certain temperature is

ISSN No:-2456-2165 https://doi.org/10.38124/ijisrt/25jul1701

capable of storing and releasing large amounts of energy. Solid liquid PCMs have a unique advantage of negligible volume expansion between solid crystalline structures along with the elimination of leaks [28].

Alot of studies have been performed on PCMs for the last three decades which are found to be very interesting due to their ability to store large amount of energy as latent heat at a constant phase transition temperature [46, 5, 39, 40]. However, some of disadvantages such as low thermal conductivity which impedes high rate of charge and discharge of heat flux were observed. The PCMs have many useful properties including heat source at constant temperature, heat recovery with small temperature drop, high storage density, melting point which matches the applications, low vapor pressure (1 bar) at the operational temperature, and chemical stability and non-corrosiveness.

The choice of PCM is based on the melting temperature, the latent heat of fusion, density and other considerations such as toxicity, corrosiveness and cost [15]. As one of the goals of latent energy storage is to achieve a high storage density in a relatively small volume, PCMs should have a high melting enthalpy kJ/Kg and a high density (Kg/m^2), that is, a high volumetric melting enthalpy [16]. No single material can have all the required properties for an ideal thermal storage media [30]. Practical difficulties include; low thermal conductivity, density change, stability of properties under extended cycling, phase segregation and sub-cooling of PCM. Among the materials for phase change are Sodium Nitrate (melting point 308^0C, density $2.26g/cm^3$, specific heat $93.05j/(molK)$) and Potassium Nitrate (melting point $334\ ^0C$, density $2.11g/cm^3$, specific heat $95.06j/(molK)$.

In order to increase thermal conductivity of a PCM, several heat transfer enhancement techniques have been studied such as incorporating high thermal conductivity enhancers such as nanoparticles into PCM and porous heat transfer media, extending heat transfer surfaces by fins and capsules, using intermediate heat transfer medium or heat pipes and employing multiple PCMs [31]. Heat transfer improves when thermal penetration depth or heat diffusion is increased. Other common enhancement techniques include addition of high thermal conductivity materials such as nanoparticles, extended surfaces, structures and heat pipes, as well as utilizing encapsulation and cascaded configurations. Combination of two or more of the aforementioned techniques, enhances heat transfer rates considerably [21].

➢ *Contribution*

The low thermal conductivity of PCMs impedes the high rate of charge and discharge of heat flux. Heat transfer enhancement techniques, such as incorporating nano-particles into PCMs, using porous heat transfer media, and employing multiple PCMs improve thermal conductivity. The choice of PCM is critical, considering factors like melting temperature, latent heat of fusion, density, toxicity, corrosiveness, and cost. The criteria for selecting PCMs, need to emphasize on the need for high volumetric melting enthalpy. This is because no single material may possess all the required properties for an ideal thermal storage medium. Practical difficulties in PCM applications such as low thermal conductivity, density change, stability under extended cycling, phase segregation, and sub-cooling. This can be addressed by achieving an ideal thermal storage medium. Thus addressing these practical difficulties is crucial for the successful implementation of PCM-based energy storage systems.

II. RELATED WORKS

The finite volume method (FVM), sometimes referred to as the control volume method, was introduced by [2], developed for solving heat transfer and fluid flow problems. FVM is a discretization technique for partial differential equations, especially those that arise from physical conservation laws, and are discretized or transformed into a set of algebraic equations that a computer can solve.

The main advantage of FVM over others like the FDM and FEM is its close connection to the underlying factors of conservation of laws (conservation of mass, conservation of energy, conservation of momentum) [37]. FVM ensures that quantities remain conserved at discrete levels; this agrees with the law of physics at all discretisation levels. It divides the domain into a finite number of non-overlapping cells or control volumes over which conservation (piecewise linear profile between any two points) is enforced in a discrete sense.

FVM can also be applied to various mesh structures and geometries [20]. It is applied in both unstructured and structured mesh quite well. Within each node in the mesh, a control volume is constructed over which the governing equations are solved discretely. The two components of discretization in FVM are the approximation of the flux through a control volume face by numerical integration over the face and the evaluation of the functions.

PCM-based thermal storage devices offer a versatile, sensible, and latent heat storage solution. They are precious in applications where temperature control, high energy density, and reduced heat loss are essential. Ongoing research and development in PCM technology will likely lead to improved materials and broader adoption in various sectors, including renewable energy, buildings, and industrial processes. For instance, [27] explores three critical parameters: fin arrangement, fin shape, and the number of fins in PCM. Among these parameters, the configuration with eight fins, where the bottom fin length increases while compensating for reduced side fin length, is the most effective. This configuration results in an impressive 60.77% reduction in the combined melting and solidification duration, showcasing its potential for enhancing the efficiency of thermal energy storage systems.

[43] introduced a hybrid sensible-latent thermal energy storage (TES) system to overcome issues with single-tank thermocline TES systems, such as quick thermocline degradation and temperature fluctuations during discharge. The study experimentally assesses the system via a combination of sensible heat concrete with axial holes and multiple layers of PCMs. Four configurations were tested: MLSPCM, SLSPCM-1, SLSPCM-2, and SSCB. Results

ISSN No:-2456-2165 https://doi.org/10.38124/ijisrt/25jul1701

indicated that MLSPCM performance was the best, with an 87% effective discharge efficiency and a storage capacity of 12.53 kWh. Using multilayers of PCM with suitable melting and solidification temperatures and cost-effective sensible concrete, this approach proved to be a viable and economical TES solution for medium-temperature applications.

[1] explored the potential of a cost-effective TES solution for medium-temperature industrial applications like chemical processing and beverages. Traditional single-tank thermocline TES systems face performance issues due to thermocline degradation during discharging. This is solved by the introduction of a novel combined sensible-latent heat configuration. It involved using structured, cost-effective, sensible heat materials with encapsulated phase change material (PCM) capsules, creating cascaded, layered, packed beds within the tank. Numerical simulations evaluated the performance of different configurations, and the results suggested that the TES system with a volume fraction arrangement of (40%-20%-40%) performance was the best, followed by (25%-50%-25%) and (10%-80%-10%), respectively. The single-layered sensible rod with PCM (SLSPCM) arrangement performance was the least effective. This approach, which involved multistage PCMs with suitable characteristics and cost-effective structured filler material, offered an efficient and economical TES alternative.

[41] explored the cascade latent heat thermal energy storage (LHTES) system by combining one unit of erythritol and two units of paraffin wax with a melting point of approximately 60^0C, effectively recovering medium-temperature industrial waste heat (150–180°C). This system addresses the limitations of single-PCM by absorbing waste heat below erythritol's melting point (around 118 °C) during charging and supplying heat above paraffin wax's melting point during discharging. Prototype testing confirmed its superior performance, increasing waste heat recovery efficiency from 15.8% to 63.4% at 100 L/h and 160°C compared to a single-stage erythritol-based system. An active discharging strategy also raised the average heat supply temperature from 37 °C (with a constant flow rate) to 53.6 °C. This highly efficient cascade LHTES system promises to decarbonize building space heating by recovering medium-temperature waste heat.

III. PROPOSED METHOD

The numerical scheme simulates the solid-liquid phase change process using mathematical models described by conservation and solving PDEs [45]. Mathematical models were derived by considering a smooth interface enthalpy method on a fixed grid and structured mesh and formulating governing equations for PCM with and without nanoparticles. FVM discretizes the domain and governing equations. This was achieved by applying the divergence theorem to convert volume integrals to surface integrals for each control volume. Function values and flux were approximated from the centre of control volumes. The PDEs obtained were thus transformed into a set of algebraic equations to be solved by MATLAB.

In physical geometry, solar energy is the source of thermal energy conveyed by hot water, transported by gravity, then stored in the PCM during the melting process as latent heat and released at an appropriate time during the solidification process. A small desirable amount of Sodium Chloride volume fractions acting as Nanoparticles is added to the PCM. A solid salt mixture of Sodium Nitrate and Potassium Nitrate mixed in the ratio of $3:2$. Heat transfer is more enhanced in large surface areas; thus, spherical shapes with a diameter of 100 nm nanoparticles are preferred for the study.

A. Models for Phase Change Process

The mathematical models are derived by assuming a smooth interface with thermal conductivity and latent heat of fusion being continuous and differentiable functions of temperature. Mathematical modelling of the phase change process is complex due to the existence of a transition region [11]. A mixture of solid and liquid phases, in which the phase change occurs, results in complex changes in transport properties such as density, specific heat, conductivity, and the latent heat of fusion, which depends on temperature. The phase transition region propagates in spatial directions (its location changes as time elapses), resulting in initial value problems containing singularities at the interfaces and challenges the numerical simulation.

- *Sharp-Interface Models*

Sharp-interface models where liquid and solid phases are assumed to be separated by infinitely thin sharp interface [14]. The transport properties such as density, specific heat and conductivity are assumed to experience a jump at the interface. The latent heat of fusion is assumed to be instantaneously released or absorbed at the interface, resulting in step (sharp) change in the transport properties, and mathematical models for liquid and solid phases are derived individually. Disadvantages of this model are that a sharp interface leads to a mathematical model in which the initial value problem contains singularity at the interface and that spatial location during evolution requires front-tracking methods.

- *Phase Field Models*

Phase field models where the solid and liquid phases are also assumed to be separated by a finite width (in temperature) transition region, where transport properties are assumed to vary with temperature between the two states [23]. The method is based on the specification of free energy density functional, which is the main driving force for the movement of the phase transition region. The models eliminate the sharp interfaces and their tracking, but alongside these, there are some disadvantages. A priori knowledge of the free energy density functional for the application at hand is required; the mathematical model cannot simulate the initiation or formation of the solid-liquid interface; hence, the liquid-solid phases and the transition region must be defined as initial conditions. This limitation is due to the specific nature of the free energy function. However, if a liquid-solid interface is specified as an initial condition, then the phase field models are quite effective in simulating the movement of the front during evolution. In most applications of interest, simulation of initiation of the transition region is important as it may not

ISSN No:-2456-2165 https://doi.org/10.38124/ijisrt/25jul1701

be possible to know its location and the precise conditions under which it initiates a priori. These limitations have resulted in minimal widespread use of these mathematical models in practical applications.

➢ *Enthalpy Approach*

The enthalpy approach is where the energy equation is recast in terms of enthalpy and temperature, keeping them as dependent variables in the mathematical model [42]. Computations of numerical solutions of the resulting initial value problem are performed on a fixed discretization. This approach eliminates the energy balance equation at the interface used in the sharp interface models and introduces a finite phase transition region (over a small temperature change) called a mushy region between the liquid and the solid phases. The transport properties are assumed to vary in some manner from one phase to the other phase. The concept of liquid or solid fraction is generally introduced to account for the mushy region being a mixture of solid and liquid phases [38]. Due to the assumption of the mushy region separating the solid and the liquid phases, the sharp interface and the associated problems, such as singularity, are inhibited, giving the approach an advantage over the others in numerical computations of the evolution of phase change problems. The Darcy law for porous media is adopted to model the flow of PCM in the mushy region [47]. The law is based on the empirical measurement of permeability and is expressed as

$$u_i = -\frac{K}{\mu}\{\frac{\partial P}{\partial x_i} - \rho g_{xi}\} \quad (3)$$

Where K is the permeability, in the case of a mushy region of commercial material, which is a function of liquid fraction; in the model, permeability decreases with decreasing liquid fraction; consequently, it forces all the velocities to become zero in the case of a stationary solid. The coefficient $\frac{K}{\mu}$ decreases from a significant value in the solid phase to zero in the liquid phase. As a result, the Darcy source term vanishes as the liquid fraction becomes 1. The mathematical models derived and presented here are the same as those in Lagrangian and Eulerian descriptions. They are based on the first law of thermodynamics using specific total energy and the heat vector augmented by the constitutive equation for the heat vector.

In this study, mathematical models are derived based on the assumption that the stress field is constant and the velocity field is zero in the solid region but nonzero in the liquid region. In the transition zone, the stress and the velocities are assumed to make the transition from a nonzero state in the fluid to a constant stress state and zero velocity in the solid phase based on the temperature with the assumption that the solid particles in the transition region form a porous medium through which the fluid flows. The enthalpy approach for the phase change is preferred, considering the space-time coupled approximation method.

B. Boundary Conditions

There are three types of boundary conditions (BC) which can be developed and imposed on the coupled governing equations to make them well-posed and solvable, namely, Dirichlet boundary condition [3], Neumann boundary condition [8] and Cauchy boundary condition [7]. In Dirichlet Boundary conditions, the value of the function is specified on the boundary, and dependent variables of the governing equations are prescribed in the domain at different points [3]. In Neumann Boundary conditions, the value of the derivative normal to the boundary is specified. A Neumann BC imposed on governing equations specifies the derivative values of a solution to be taken on the boundary of the domain [8]. In Cauchy Boundary conditions, the values involve a linear combination of Dirichlet and Neumann BC to governing equations [7]. A Cauchy BC imposed on governing equations specifies both the values of a solution of a differential equation to take on the domain and the normal derivation at the boundary.

The PCM is enclosed within annular cavity formed between two concentric horizontal cylindrical shells with the inner shell considered to be of a significantly thinned wall subjected to a constant heat flux of 225 ^{0}C (1 ^{0}C higher than the melting point of the PCM) on the southern wall keeping the outer shell (northern wall) at adiabatic condition which simulates the PCM storing thermal energy during charging. The inlet velocity of the melt is 0.003cm/s. The western and eastern walls are also kept at adiabatic condition. The elementary cross-sectional cavity of dimension 10cm (x direction) by 1cm (y direction) is used to model the phase change process as represented by the Fig. 2.

ISSN No:-2456-2165 https://doi.org/10.38124/ijisrt/25jul1701

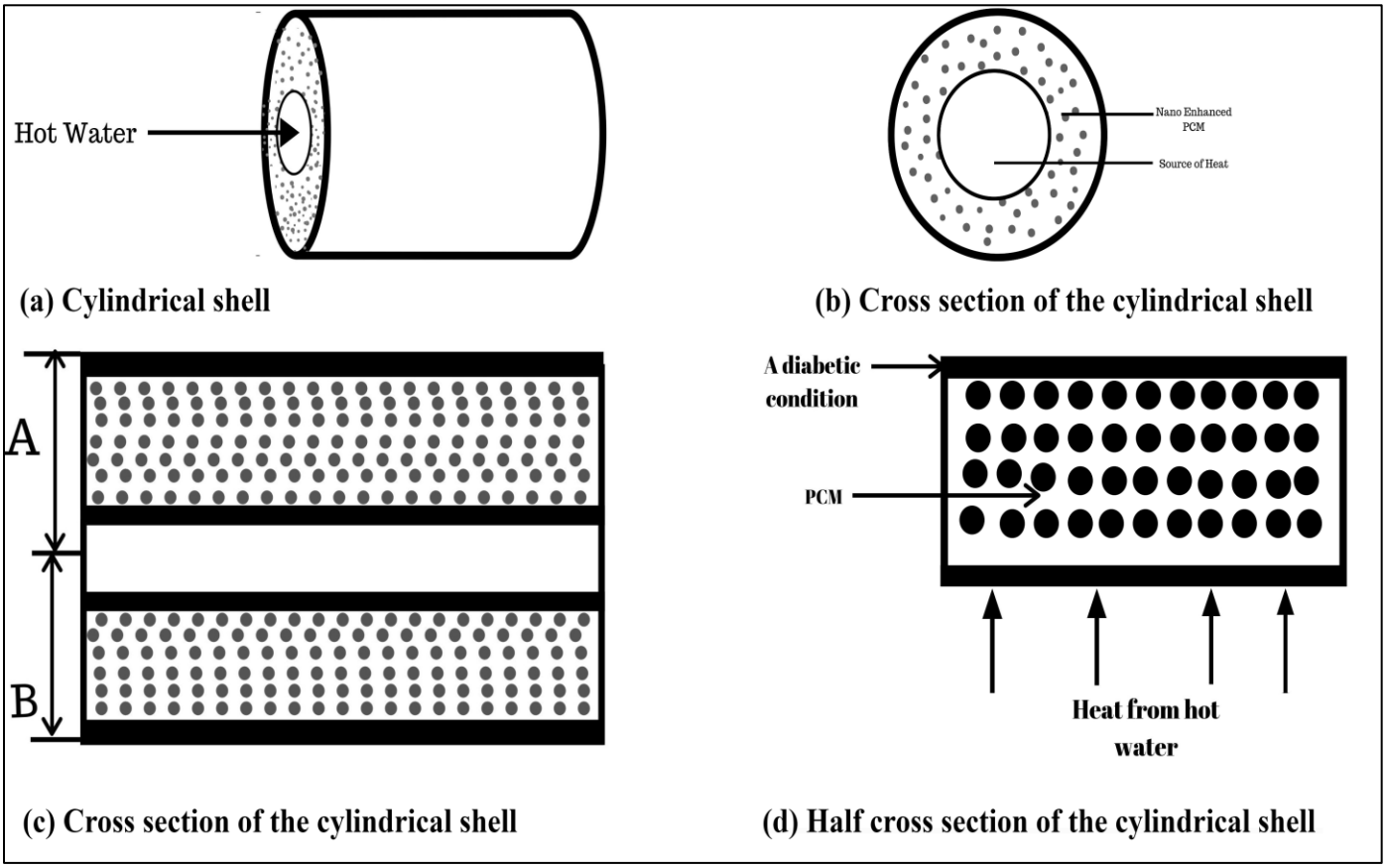

Fig 2 The Elementary Cross-Sectional Cavity of Dimension 10cm (x Direction) by 1cm (y Direction) is used to Model the phase Change Process

C. Discretization of the Partial Differential Equations

FVM is derived based on the integral form of conservation laws. It discretizes the domain into finite control volumes and approximates the total integral of flux over each control volume rather than pointwise approximations at mesh points (see Figure 2). These values are modified on each time step by using the flux through the edges of the grid cells. Discretization of governing equations follows three steps: Space discretization, Time discretization and Equation discretization. Space discretization involves the definition of a numerical grid, which replaces the continuous space with a finite number of discrete elements with computational points at their centroids. At these points, the solution of dependent variables is computed. This process is termed grid generation. Time discretization assumes the division of the entire time interval into a finite number of small sub-intervals, called time steps, which guarantee convergence of the solution. Discretization of equations involves the replacement of the individual terms in the governing equations by algebraic expressions connecting the variable values at computational points in the grid.

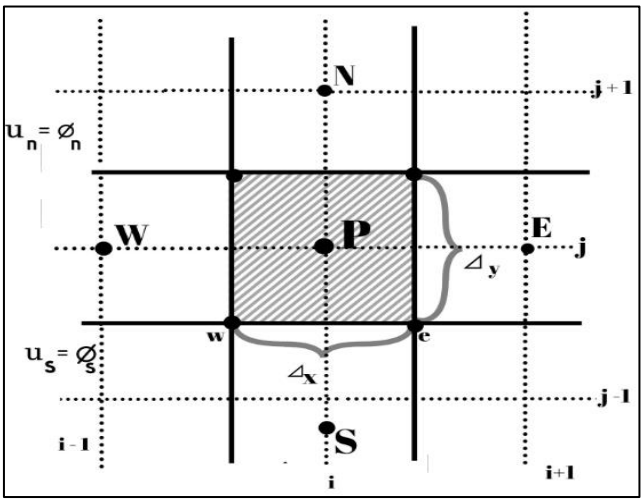

Fig 3 Control Volume

D. Non-Dimensionlization and Discretization of the Governing Equations

Non-dimensionlisation is the partial or full removal of physical dimensions from an equation involving physical quantities by a suitable substitution of variables. Reynold's Number being one of the dimensionless number gives a measure of the ratio of inertia(resistant to change or motion) forces to viscous forces. Laminar flows occurs at low Reynolds's Number whereas turbulent flow occurs at high Reynold's number. The following variables are used to non-dimensionalization of the parameters: time, distance, velocity, temperature and pressure as:

ISSN No:-2456-2165 https://doi.org/10.38124/ijisrt/25jul1701

$t^* = \frac{t}{L/U_\infty}$, $x^* = \frac{x}{L}$, $y^* = \frac{y}{L}$, $z^* = \frac{z}{L}$, $u^* = \frac{u}{U_\infty}$, $v^* = \frac{v}{U_\infty}$, $w^* = \frac{w}{U_\infty}$, $p^* = \frac{p-p_\infty}{\rho/U_\infty^2}$, $T^* = \frac{T-T_\infty}{\Delta T}$.

E. Non Dimensionlisation and Discretiastion of Conservation of Mass Equation

The flow of molten PCM is governed by continuity equation and momentum equations expressed in cartesian coordinates. Non dimesionlising, we obtain

$$\nabla = i\frac{\partial}{\partial x} + j\frac{\partial}{\partial y} + k\frac{\partial}{\partial z} \tag{4}$$

$$\vec{V} = ui + vj + wk \tag{5}$$

$$\nabla \cdot \vec{V} = \frac{\partial u}{\partial x} + \frac{\partial v}{\partial y} + \frac{\partial w}{\partial z} \tag{6}$$

In 2-Dimensional, Equation 6 becomes,

$$\nabla \cdot \vec{V} = \frac{\partial u}{\partial x} + \frac{\partial v}{\partial y} = 0 \tag{7}$$

Non-Dimesionlizing yields

$$\frac{\partial u^* U_\infty}{\partial x^* L} + \frac{\partial v^* U_\infty}{\partial y^* L} = 0 \tag{8}$$

$$\frac{U_\infty}{L}\{\frac{\partial u^*}{\partial x^*} + \frac{\partial v^*}{\partial y^*}\} = 0 \tag{9}$$

$$\frac{\partial u^*}{\partial x^*} + \frac{\partial v^*}{\partial y^*} = 0 \tag{10}$$

Discretisation of conservation of mass equation

$$\int_{y_{(j-\frac{1}{2})}}^{y_{(j+\frac{1}{2})}} \int_{x_{(i-\frac{1}{2})}}^{x_{(i+\frac{1}{2})}} \frac{\partial u^*}{\partial x^*} dxdy + \int_{y_{(j-\frac{1}{2})}}^{y_{(j+\frac{1}{2})}} \int_{x_{(i-\frac{1}{2})}}^{x_{(i+\frac{1}{2})}} \frac{\partial v^*}{\partial y^*} dxdy = 0 \tag{11}$$

$$\int_{y_{(j-\frac{1}{2})}}^{y_{(j+\frac{1}{2})}} \int_{x_{(i-\frac{1}{2})}}^{x_{(i+\frac{1}{2})}} \frac{\partial u^*}{\partial x^*} dxdy + \int_{y_{(j-\frac{1}{2})}}^{y_{(j+\frac{1}{2})}} \int_{x_{(i-\frac{1}{2})}}^{x_{(i+\frac{1}{2})}} \frac{\partial v^*}{\partial y^*} dxdy\} = 0 \tag{12}$$

$$\Delta t \, \Delta y \int_{x_{(i-\frac{1}{2})}}^{x_{(i+\frac{1}{2})}} \frac{\partial u^*}{\partial x^*} dx + \Delta t \, \Delta x \int_{y_{(j-\frac{1}{2})}}^{y_{(j+\frac{1}{2})}} \frac{\partial v^*}{\partial y^*} dy = 0 \tag{13}$$

$$\Delta t \, \Delta y(u^*_{(i+\frac{1}{2})} - u^*_{(i-\frac{1}{2})}) + \Delta t \, \Delta x(v^*_{(j+\frac{1}{2})} - v^*_{(j-\frac{1}{2})}) = 0 \tag{14}$$

$$\Delta y \, \Delta t\{(\frac{u^*_{i+1}+u^*_i}{2}) - (\frac{u^*_{i-1}+u^*_i}{2})\} + \Delta x \, \Delta t\{(\frac{v^*_{j+1}+v^*_j}{2}) - (\frac{v^*_{j-1}+v^*_j}{2})\} = 0 \tag{15}$$

$$\frac{\Delta t \Delta y}{2}(u^*_{i+1} - u^*_{i-1}) + \frac{\Delta x \Delta t}{2}(v^*_{j+1} - v^*_{j-1}) = 0 \tag{16}$$

Simplifying further we obtain,

$$\Delta y(u^*_{i+1} - u^*_{i-1}) + \Delta x(v^*_{j+1} - v^*_{j-1}) = 0 \tag{17}$$

F. Non Dimesionlization of Momentum Equations

Non dimensionlizing Equation 5, momentum equation in x-direction using the given variables

$$t^* = \frac{t}{\frac{L}{U_\infty}} \Rightarrow \frac{\partial t^*}{\partial t} = \frac{U_\infty}{L} \text{ and } t = \frac{t^* L}{U_\infty}$$

Substituting with values of u and t in $\frac{\partial u}{\partial t}$, we obtain

ISSN No:-2456-2165 https://doi.org/10.38124/ijisrt/25jul1701

$$\frac{\partial u}{\partial t} = \frac{U_\infty^2}{L}\frac{\partial u^*}{\partial t^*} \tag{18}$$

$$x = x^*L \Rightarrow \frac{\partial x^*}{\partial x} = \frac{1}{L},\ y = y^*L \Rightarrow \frac{\partial y^*}{\partial y} = \frac{1}{L},\ u = u^*U_\infty \Rightarrow \frac{\partial u^*}{\partial x} = 0$$

$$\frac{\partial u}{\partial x} = \frac{\partial (u^*U_\infty)}{\partial x^*}\frac{\partial x^*}{\partial x} = U_\infty \frac{\partial u^*}{\partial x^*}\frac{1}{L} = \frac{U_\infty}{L}\frac{\partial u^*}{\partial x^*} \tag{19}$$

$$\frac{\partial u}{\partial y} = \frac{\partial (u^*U_\infty)}{\partial y^*}\frac{\partial y^*}{\partial y} = U_\infty \frac{\partial u^*}{\partial y^*}\frac{1}{L} = \frac{U_\infty}{L}\frac{\partial u^*}{\partial y^*} \tag{20}$$

We know $\frac{\partial}{\partial x} = \frac{\partial}{\partial x^*}\frac{\partial x^*}{\partial x}$, $\frac{\partial x^*}{\partial x} = \frac{1}{L}$, $\frac{\partial u}{\partial x} = \frac{U_\infty}{L}\frac{\partial u^*}{\partial x^*}$ then we obtain,

$$\frac{\partial^2 u}{\partial x^2} = \frac{\partial}{\partial x}\left(\frac{\partial u}{\partial x}\right) = \frac{\partial}{\partial x^*}\frac{\partial x^*}{\partial x}\left(\frac{U_\infty}{L}\frac{\partial u^*}{\partial x^*} = \frac{U_\infty}{L^2}\frac{\partial^2 u^*}{\partial x^{*2}}\right. \tag{21}$$

We also know $\frac{\partial}{\partial y} = \frac{\partial}{\partial y^*}\frac{\partial y^*}{\partial y}$, $\frac{\partial y^*}{\partial y} = \frac{1}{L}$, $\frac{\partial u}{\partial y} = \frac{U_\infty}{L}\frac{\partial u^*}{\partial y^*}$ then we obtain,

$$\frac{\partial^2 u}{\partial y^2} = \frac{\partial}{\partial y}\left(\frac{\partial u}{\partial y}\right) = \frac{\partial}{\partial y^*}\frac{\partial y^*}{\partial y}\left(\frac{U_\infty}{L}\frac{\partial u^*}{\partial y^*} = \frac{U_\infty}{L^2}\frac{\partial^2 u^*}{\partial y^{*2}}\right. \tag{22}$$

Substituting equations 23-27 in the momentum equation 5, we obtain,

$$\rho\left(\frac{U_\infty^2}{L}\frac{\partial u^*}{\partial t^*} + u^*U_\infty\frac{U_\infty}{L}\frac{\partial u^*}{\partial x^*} + v^*U_\infty\frac{U_\infty}{L}\frac{\partial u^*}{\partial y^*}\right) = \mu\left(\frac{U_\infty}{L^2}\frac{\partial^2 u^*}{\partial x^{*2}} + \frac{U_\infty}{L^2}\frac{\partial^2 u^*}{\partial y^{*2}}\right) \tag{23}$$

Multiply through by $\frac{L}{\rho U_\infty^2}$, we obtain

$$\left(\frac{\partial u^*}{\partial t^*} + u^*\frac{\partial u^*}{\partial x^*} + v^*\frac{\partial u^*}{\partial y^*}\right) = \frac{\mu}{\rho L U_\infty}\left(\frac{\partial^2 u^*}{\partial x^{*2}} + \frac{\partial^2 u^*}{\partial y^{*2}}\right) \tag{24}$$

Equating Equation 39 to 0 , we obtain

$$\left(\frac{\partial u^*}{\partial t^*} + u^*\frac{\partial u^*}{\partial x^*} + v^*\frac{\partial u^*}{\partial y^*}\right) - \frac{\mu}{\rho L U_\infty}\left(\frac{\partial^2 u^*}{\partial x^{*2}} + \frac{\partial^2 u^*}{\partial y^{*2}}\right) = 0 \tag{25}$$

Which is the Non-dimensionlised momentum equation in x direction and $\frac{\mu}{\rho L U_\infty} = \frac{1}{Re}$

G. Discretisation of Momentum Equations in x Direction

Equation 30 is discritised as follows,

$$\int_{t_k}^{t_{k+1}}\int_{y_{(j-\frac{1}{2})}}^{y_{(j+\frac{1}{2})}}\int_{x_{(i-\frac{1}{2})}}^{x_{(i+\frac{1}{2})}}\left\{\frac{\partial u^*}{\partial t^*} + u^*\frac{\partial u^*}{\partial x^*} + v^*\frac{\partial u^*}{\partial y^*} - \frac{\mu}{\rho L U_\infty}\left[\frac{\partial^2 u^*}{\partial x^{*2}} + \frac{\partial^2 u^*}{\partial y^{*2}}\right\}dxdydt\right. \tag{26}$$

Integrating different parts of Equation (31) we obtain,

$$\int_{t_k}^{t_{k+1}}\int_{y_{(j-\frac{1}{2})}}^{y_{(j+\frac{1}{2})}}\int_{x_{(i-\frac{1}{2})}}^{x_{(i+\frac{1}{2})}}\frac{\partial u^*}{\partial t^*}dxdydt = \Delta x\,\Delta y[(u_{k+1} - (u_k)] \tag{27}$$

Replacement of original 34 has been done below 15.5.21(ignore the statement) rephrase

$$\int_{t_{(k)}}^{t_{k+1}}\int_{y_{(j-\frac{1}{2})}}^{y_{(j+\frac{1}{2})}}\int_{x_{(i-\frac{1}{2})}}^{x_{(i+\frac{1}{2})}}u^*\frac{\partial u^*}{\partial x^*}dxdydt = \Delta y\,\Delta t u_i^*(u^*_{((i+\frac{1}{2})} - u^*_{(i-\frac{1}{2})} = \Delta y\,\Delta t u_i^*\{(\frac{u^*_{i+1}+u^*_i}{2}) - (\frac{u^*_i+u^*_{i-1}}{2})\} = \frac{\Delta y\Delta t}{2}u_i^*(u^*_{i+1} - u^*_{i-1}) = 0.5Au_i^*(u^*_{i+1} - u^*_{i-1}) \tag{28}$$

$$\int_{t_{(k)}}^{t_{k+1}}\int_{y_{(j-\frac{1}{2})}}^{y_{(j+\frac{1}{2})}}\int_{x_{(i-\frac{1}{2})}}^{x_{(i+\frac{1}{2})}}v^*\frac{\partial u^*}{\partial y^*}dxdydt = \Delta x\,\Delta t v_j^*(u^*_{((j+\frac{1}{2})} - u^*_{(j-\frac{1}{2})}) = \Delta x\,\Delta t v_j^*\{(\frac{u^*_{j+1}+u^*_j}{2}) - (\frac{u^*_j+u^*_{j-1}}{2})\} = \frac{\Delta x\,\Delta t}{2}v_j^*(u^*_{j+1} - u^*_{j-1}) = 0.5Bv_j^*(u^*_{j+1} - u^*_{j-1}) \tag{29}$$

ISSN No:-2456-2165 https://doi.org/10.38124/ijisrt/25jul1701

$$\int_{t(k)}^{t(k+1)}\int_{y_{(j-\frac{1}{2})}}^{y_{(j+\frac{1}{2})}}\int_{x_{(i-\frac{1}{2})}}^{x_{(i+\frac{1}{2})}}\frac{\partial^2 u^*}{\partial x^{*2}}dxdydt = \Delta y \Delta t\frac{du^*}{dx^*}\Big|_{(i-\frac{1}{2})}^{(i+\frac{1}{2})} = \Delta y \Delta t(\frac{du^*}{dx^*}|_{(i+\frac{1}{2})} - \frac{du^*}{dx^*}|_{(i-\frac{1}{2})}) = \Delta y \Delta t\{(\frac{u^*_{i+1}-u^*_i}{\Delta x}) - (\frac{u^*_i-u^*_{i-1}}{\Delta x} = \Delta y \Delta t(\frac{u^*_{i+1}-2u^*_i+u^*_{i-1}}{\Delta x}) = \frac{\Delta y \Delta t}{\Delta x}(u^*_{i+1} - 2u^*_i + u^*_{i-1}) = Q(u^*_{i+1} - 2u^*_i + u^*_{i-1}) \quad (30)$$

$$\int_{t(k)}^{t(k+1)}\int_{y_{(j-\frac{1}{2})}}^{y_{(j+\frac{1}{2})}}\int_{x_{(i-\frac{1}{2})}}^{x_{(i+\frac{1}{2})}}\frac{\partial^2 u^*}{\partial y^{*2}}dxdydt = \Delta x \Delta t\frac{du^*}{dy^*}\Big|_{(j-\frac{1}{2})}^{(j+\frac{1}{2})} = \Delta x \Delta t(\frac{du^*}{dy^*}|_{(j+\frac{1}{2})} - \frac{du^*}{dy^*}|_{(j-\frac{1}{2})}) \quad = \Delta x \Delta t\{(\frac{u^*_{j+1}-u^*_j}{\Delta y}) - (\frac{u^*_j-u^*_{j-1}}{\Delta y}) = \Delta x \Delta t(\frac{u^*_{j+1}-2u^*_j+u^*_{j-1}}{\Delta y})\} = \frac{\Delta x \Delta t}{\Delta y}(u^*_{j+1} - 2u^*_j + u^*_{j-1}) = R(u^*_{j+1} - 2u^*_j + u^*_{j-1}) \quad (31)$$

Where $A = \Delta y \Delta t$, $B = \Delta x \Delta t$, $C = \Delta y \Delta x$, $Q = \frac{\Delta y \Delta t}{\Delta x}$, $R = \frac{\Delta x \Delta t}{\Delta y}$.

Combining equations from 28 to 31 , we obtain discretised momentum equation in x direction as

$$C[(u_{(k+1))} - (u_{(k)})] + 0.5Au_i^*(u^*_{(i+1)} - u^*_{(i-1)}) + 0.5Bv_j^*(u^*_{(j+1)} - u^*_{(j-1)}) - \frac{\mu}{\rho L U_\infty}\{Q(u^*_{i+1} - 2u^*_i + u^*_{i-1}) + R(u^*_{j+1} - 2u^*_j + u^*_{j-1})\} = 0 \quad (32)$$

Applying Picards Linearisation method to the non linear equation (34) and simplifying it by dropping * which symbolised non-dmensionlised terms we obtain

$$C[u_{k+1} - u_k] + 0.5A\bar{u}_i(u_{(i+1)} - u_{(i-1)}) + 0.5B\bar{v}_j(u_{(j+1)} - u_{(j-1)}) - \frac{\mu_{nf}}{\rho_{nf} L U_\infty}\{Q(u_{i+1} - 2u_i + u_{i-1}) + R(u_{j+1} - 2u_j + u_{j-1})\} = 0 \quad (33)$$

$$\mu_{nf} = \frac{\mu_{PCM}}{(1-\phi)^{2.5}} \quad (34)$$

Where ϕ is the volume fraction of nanoparticles, μ_{PCM} is the dynamic viscosity of pure PCM, and μ_{nf} is the dynamic viscosity of NEPCMs.

H. Non Dimensionlization of Momentum Equations in y Direction

Non dimensionlizing equation 6, momentum equation in y-direction using the given variables

$$x = x^*L \Rightarrow \frac{\partial x^*}{\partial x} = \frac{1}{L}, y = y^*L \Rightarrow \frac{\partial y^*}{\partial y} = \frac{1}{L}, v = v^*U_\infty \Rightarrow \frac{\partial v^*}{\partial x} = 0, T^* = \frac{T-T_\infty}{\triangle T} \Rightarrow T = T^* \triangle T + T_\infty, t^* = \frac{t}{L/U_\infty} \Rightarrow t^* = \frac{tU_\infty}{L} \Rightarrow \frac{\partial t^*}{\partial t} = \frac{U_\infty}{L}, \Rightarrow \frac{\partial v}{\partial t} = U_\infty \frac{\partial v^*}{\partial t^*}\frac{U_\infty}{L}$$

$$\frac{\partial v}{\partial t} = \frac{U_\infty^2}{L}\frac{\partial v^*}{\partial t^*} \quad (35)$$

$$\frac{\partial v}{\partial x} = \frac{\partial(v^*U_\infty)}{\partial x^*}\frac{\partial x^*}{\partial x} = U_\infty \frac{\partial v^*}{\partial x^*}\frac{1}{L} = \frac{U_\infty}{L}\frac{\partial v^*}{\partial x^*} \quad (36)$$

$$\frac{\partial v}{\partial y} = \frac{\partial(v^*U_\infty)}{\partial y^*}\frac{\partial y^*}{\partial y} = U_\infty \frac{\partial v^*}{\partial y^*}\frac{1}{L} = \frac{U_\infty}{L}\frac{\partial v^*}{\partial y^*} \quad (37)$$

$$\frac{\partial^2 v}{\partial x^2} = \frac{\partial}{\partial x}(\frac{\partial v}{\partial x}) = \frac{\partial}{\partial x}(\frac{U_\infty}{L}\frac{\partial v^*}{\partial x^*}) \quad (38)$$

We know $\frac{\partial}{\partial x} = \frac{\partial}{\partial x^*}\frac{\partial x^*}{\partial x}$, $\frac{\partial x^*}{\partial x} = \frac{1}{L}$, $\frac{\partial v}{\partial x} = \frac{U_\infty}{L}\frac{\partial v^*}{\partial x^*}$ then we obtain,

$$\frac{\partial^2 v}{\partial x^2} = \frac{\partial}{\partial x}(\frac{\partial v}{\partial x}) = \frac{\partial}{\partial x^*}\frac{\partial x^*}{\partial x}(\frac{U_\infty}{L}\frac{\partial v^*}{\partial x^*} = \frac{U_\infty}{L^2}\frac{\partial^2 v^*}{\partial x^{*2}} \quad (39)$$

We know $\frac{\partial}{\partial y} = \frac{\partial}{\partial y^*}\frac{\partial y^*}{\partial y}$, $\frac{\partial y^*}{\partial y} = \frac{1}{L}$, $\frac{\partial v}{\partial y} = \frac{U_\infty}{L}\frac{\partial v^*}{\partial y^*}$ then we obtain,

$$\frac{\partial^2 v}{\partial y^2} = \frac{\partial}{\partial y}(\frac{\partial v}{\partial y}) = \frac{\partial}{\partial y^*}\frac{\partial y^*}{\partial y}(\frac{U_\infty}{L}\frac{\partial v^*}{\partial y^*} = \frac{U_\infty}{L^2}\frac{\partial^2 v^*}{\partial y^{*2}} \quad (40)$$

Substituting equations from (37-40) in Equation 6 we obtain,

$$\rho(\frac{U_\infty^2}{L}\frac{\partial v^*}{\partial t^*} + u^*U_\infty\frac{U_\infty}{L}\frac{\partial v^*}{\partial x^*} + v^*U_\infty\frac{U_\infty}{L}\frac{\partial v^*}{\partial y^*}) = \mu(\frac{U_\infty}{L^2}\frac{\partial^2 v^*}{\partial x^{*2}} + \frac{U_\infty}{L^2}\frac{\partial^2 v^*}{\partial y^{*2}}) + \beta\rho g(T^* \triangle T + T_\infty - T_r) \quad (41)$$

Simplyfying further, Multiply through by $\frac{L}{\rho U_\infty^2}$

ISSN No:-2456-2165 https://doi.org/10.38124/ijisrt/25jul1701

$$(\frac{\partial v^*}{\partial t^*} + v^* \frac{\partial v^*}{\partial x^*} + v^* \frac{\partial v^*}{\partial y^*}) = \frac{\mu}{\rho L U_\infty} (\frac{\partial^2 v^*}{\partial x^{*2}} + \frac{\partial^2 v^*}{\partial y^{*2}}) + \frac{L}{U_\infty^2} \beta g (T^* \Delta T + T_\infty - T_r) \quad (42)$$

Rearranging equation 53 , we obtain non dimensionlised momentum equation in y direction

$$(\frac{\partial v^*}{\partial t^*} + u^* \frac{\partial v^*}{\partial x^*} + v^* \frac{\partial v^*}{\partial y^*}) - \frac{\mu}{\rho L U_\infty} (\frac{\partial^2 v^*}{\partial x^{*2}} + \frac{\partial^2 v^*}{\partial y^{*2}}) - \frac{L}{U_\infty^2} \beta g (T^* \Delta T + T_\infty - T_r) = 0 \quad (43)$$

I. Discretisation of momentum equations in y direction

Equation 43 is discritised as follows,

$$\int_{t(k)}^{t(k+1)} \int_{y_{(j-\frac{1}{2})}}^{y_{(j+\frac{1}{2})}} \int_{x_{(i-\frac{1}{2})}}^{x_{(i+\frac{1}{2})}} \{\frac{\partial v^*}{\partial t^*} + u^* \frac{\partial v^*}{\partial x^*} + v^* \frac{\partial v^*}{\partial y^*} - \frac{\mu}{\rho L U_\infty} [\frac{\partial^2 v^*}{\partial x^{*2}} + \frac{\partial^2 v^*}{\partial y^{*2}}] - \frac{L}{U_\infty^2} \beta g (T^* \Delta T + T_\infty - T_r)\} dx dy dt \quad (44)$$

Integrating different parts of Equation (46) we obtain,

$$\int_{t(k)}^{t(k+1)} \int_{y_{(j-\frac{1}{2})}}^{y_{(j+\frac{1}{2})}} \int_{x_{(i-\frac{1}{2})}}^{x_{(i+\frac{1}{2})}} \frac{\partial v^*}{\partial t^*} dx dy dt = \Delta x \Delta y [(v_{(k+1))} - (v_{(k)})] \quad (45)$$

$$\int_{t(k)}^{t(k+1)} \int_{y_{(j-\frac{1}{2})}}^{y_{(j+\frac{1}{2})}} \int_{x_{(i-\frac{1}{2})}}^{x_{(i+\frac{1}{2})}} u_i^* \frac{\partial v^*}{\partial x^*} dx dy dt = \Delta y \Delta t u_i^* (v^*_{((i+\frac{1}{2})} - v^*_{(i-\frac{1}{2})}) = \Delta y \Delta t u_i^* \{(\frac{v^*_{i+1} + v^*_i}{2}) - (\frac{v^*_i + v^*_{i-1}}{2})\} = \frac{\Delta y \Delta t}{2} u_i^* (v^*_{(i+1)} - v^*_{(i-1)}) = 0.5 A u_i^* (v^*_{(i+1)} - v^*_{(i-1)}) \quad (46)$$

Replacement of original (45) is done as follows

$$\int_{t(k)}^{t(k+1)} \int_{y_{(j-\frac{1}{2})}}^{y_{(j+\frac{1}{2})}} \int_{x_{(j-\frac{1}{2})}}^{x_{(j+\frac{1}{2})}} v_j^* \frac{\partial v^*}{\partial y^*} dx dy dt = \Delta x \Delta t v_j^* (v^*_{((j+\frac{1}{2})} - v^*_{(j-\frac{1}{2})}) = \Delta x \Delta t v_j^* \{(\frac{v^*_{j+1} + v^*_j}{2}) - (\frac{v^*_j + v^*_{j-1}}{2})\} = \frac{\Delta y \Delta t}{2} v_j^* (v^*_{(j+1)} - v^*_{(j-1)}) = 0.5 B v_j^* (v^*_{(j+1)} - v^*_{(j-1)}) \quad (47)$$

$$\int_{t(k)}^{t(k+1)} \left[\int_{y_{(j-\frac{1}{2})}}^{y_{(j+\frac{1}{2})}} \int_{x_{(i-\frac{1}{2})}}^{x_{(i+\frac{1}{2})}} \frac{\partial^2 v^*}{\partial x^{*2}} dx dy dt = \Delta y \Delta t \frac{dv^*}{dx^*} \Big|_{(i-\frac{1}{2})}^{(i+\frac{1}{2})} = \Delta y \Delta t (\frac{dv^*}{dx^*}\Big|_{(i+\frac{1}{2})} - \frac{dv^*}{dx^*}\Big|_{(i-\frac{1}{2})}) = \Delta y \Delta t \{(\frac{v^*_{i+1} - v^*_i}{\Delta x}) - (\frac{v^*_i - v^*_{i-1}}{\Delta x} = \Delta y \Delta t (\frac{v^*_{i+1} - 2v^*_i + v^*_{i-1}}{\Delta x}) = \frac{\Delta y \Delta t}{\Delta x} (v^*_{i+1} - 2v^*_i + v^*_{i-1}) = Q(v^*_{i+1} - 2v^*_i + v^*_{i-1}) \quad (48)$$

$$\int_{t(k)}^{t(k+1)} \int_{y_{(j-\frac{1}{2})}}^{y_{(j+\frac{1}{2})}} \int_{x_{(i-\frac{1}{2})}}^{x_{(i+\frac{1}{2})}} \frac{\partial^2 v^*}{\partial y^{*2}} dx dy dt = \Delta x \Delta t \frac{dv^*}{dy^*} \Big|_{(j-\frac{1}{2})}^{(j+\frac{1}{2})} = \Delta x \Delta t \left(\frac{dv^*}{dy^*}\Big|_{(j+\frac{1}{2})} - \frac{dv^*}{dy^*}\Big|_{(j-\frac{1}{2})}\right) = \Delta x \Delta t \{(\frac{v^*_{j+1} - v^*_j}{\Delta y}) - (\frac{v^*_j - v^*_{j-1}}{\Delta y}) = \Delta x \Delta t (\frac{u^*_{j+1} - 2v^*_j + v^*_{j-1}}{\Delta y})\} = \frac{\Delta x \Delta t}{\Delta y} (v^*_{j+1} - 2v^*_j + v^*_{j-1}) = R(v^*_{j+1} - 2v^*_j + v^*_{j-1}) \quad (49)$$

$$\int_{t(k)}^{t(k+1)} \int_{y_{(j-\frac{1}{2})}}^{y_{(j+\frac{1}{2})}} \int_{x_{(i-\frac{1}{2})}}^{x_{(i+\frac{1}{2})}} \frac{L}{U_\infty^2} \beta g (T^* \Delta T + T_\infty - T_r) dx dy dt = \Delta x \Delta y \Delta t \{\frac{L}{U_\infty^2} \beta g ((T^* \Delta T + T_\infty) - T_r)\} \quad (50)$$

Assembling equations from (45) to (50) together , substituting for $D = \Delta t \Delta x \Delta y$, Applying Picards Linearisation, and discarding * we obtain,

$$C[(v_{k+1} - v_k)] + 0.5 A \bar{u}_j (v_{i+1} - v_{i-1}) + 0.5 B \bar{v}_j (v_{j+1} - v_{j-1}) - \frac{\mu}{\rho_{nf} L U_\infty} \{Q(v_{i+1} - 2v_i + v_{i-1}) + R(v_{j+1} - 2v_j + v_{j-1}\} \quad -D \frac{L}{U_\infty^2} \beta g ((T_j \Delta T + T_\infty) - T_r) = 0 \quad (51)$$

J. Non Dimesionlisation and Discretisation of Conservation of Energy Equation

In equation of conservation of energy. The enthalpy H of PCMs is defined as,

$$H = C_p (T - T_r) + f_l L \quad (52)$$

Where f_l is the PCM liquid fraction and L is the latent heat of the PCMs. By caculating the enthalpy H of PCMs, the liquid fraction and temperature can be updated by the following equations.

$$f_1 = \begin{cases} 0, & H \le H_s \\ \frac{H - H_s}{H_l - H_s}, & H_s \le H < H_l \\ 1, & H \ge H_s \end{cases} \quad (53)$$

ISSN No:-2456-2165 https://doi.org/10.38124/ijisrt/25jul1701

$$T = \begin{cases} T = \frac{H_s - H}{c_p}, & H \le H_s \\ T_m, & H_s < H < H \\ T + \frac{H_s - H}{c_p}, & H \le H_s \end{cases} \quad (54)$$

➢ *Non-Dimensionlisation of Conservation of Energy Equation*

$$\frac{\partial(\rho H}{\partial t^* L/U_\infty}) + \rho c_p[u^* U_\infty \frac{\partial(T^* \Delta T + T_\infty)}{L\partial x^*} + v^* U_\infty \frac{(T^* \Delta T + T_\infty)}{L\partial y^*}] = k[\frac{\partial^2(T^* \Delta T + T_\infty)}{L\partial x^{*2}} + \frac{\partial^2(T^* \Delta T + T_\infty)}{L\partial y^{*2}}] \quad (55)$$

$$\frac{U_\infty}{L}\frac{\partial(\rho H)}{\partial t^*} + \rho c_p[u^* \frac{U_\infty}{L}\frac{\partial(T^* \Delta T + T_\infty)}{\partial x^*} + v^* \frac{U_\infty}{L}\frac{(T^* \Delta T + T_\infty)}{\partial y^*}] = \frac{k}{L}[\frac{\partial^2(T^* \Delta T + T_\infty)}{\partial x^{*2}} + \frac{\partial^2(T^* \Delta T + T_\infty)}{\partial y^{*2}}] \quad (56)$$

Multiply by $\frac{L}{U_\infty}$, and taking $T_\infty = 0$, we obtain,

$$\frac{\partial(\rho H)}{\partial t^*} + \rho c_p[u^* \frac{\partial(T^* \Delta T)}{\partial x^*} + v^* \frac{\partial(T^* \Delta T)}{\partial y^*}] = \frac{k}{U_\infty}[\frac{\partial^2(T^* \Delta T)}{\partial x^{*2}} + \frac{\partial^2(T^* \Delta T)}{\partial y^{*2})}] \quad (57)$$

Multiply by (58) $\frac{1}{\Delta T}$ we obtain,

$$\frac{1}{\Delta T}\frac{\partial(\rho H)}{\partial t^*} + \rho c_p[u^* \frac{\partial T^*}{\partial x^*} + v^* \frac{\partial T^*}{\partial y^*}] = \frac{k}{U_\infty}[\frac{\partial^2 T^*}{\partial x^{*2}} + \frac{\partial^2 T^*}{\partial y^{*2}}] \quad (58)$$

Discretisation of conservation of Energy Equations

$$\int_{t(k)}^{t(k+1)} \int_{y_{(j-\frac{1}{2})}}^{y_{(j+\frac{1}{2})}} \int_{x_{(i-\frac{1}{2})}}^{x_{(i+\frac{1}{2})}} \left[\frac{1}{\Delta T}\frac{\partial H^*}{\partial t^*} + \rho C_p u^* \frac{\partial T^*}{\partial x^*} + \rho C_p v^* \frac{\partial T^*}{\partial y^*}\right] dxdydt = \frac{k}{U_\infty}\int_{t(k)}^{t(k+1)} \int_{y_{(j-\frac{1}{2})}}^{y_{(j+\frac{1}{2})}} \int_{x_{(i-\frac{1}{2})}}^{x_{(i+\frac{1}{2})}} [\frac{\partial^2 T^*}{\partial x^{*2}} + \frac{\partial^2 T^*}{\partial y^{*2}}]dxdydt \quad (59)$$

Integrating separate components of Equation (59), we obtain,

$$\frac{1}{\Delta T}\int_{t(k)}^{t(k+1)} \int_{y_{(j-\frac{1}{2})}}^{y_{(j+\frac{1}{2})}} \int_{x_{(i-\frac{1}{2})}}^{x_{(i+\frac{1}{2})}} \frac{\partial H^*}{\partial t^*} dxdydt = \frac{\Delta x \Delta y}{\Delta T}\{H_{k+1} - H_k\} \quad (60)$$

$$\int_{t(k)}^{t(k+1)} \int_{y_{(j-\frac{1}{2})}}^{y_{(j+\frac{1}{2})}} \int_{x_{(i-\frac{1}{2})}}^{x_{(i+\frac{1}{2})}} u_i^* \frac{\partial T^*}{\partial x^*} dxdydt = \Delta y \Delta t u_i^*(T^*_{((i+\frac{1}{2})} - T^*_{(i-\frac{1}{2})}) = \Delta y \Delta t u_i^*\{(\frac{T^*_{i+1} - T^*_i}{2}) - (\frac{T^*_i - T^*_{i-1}}{2})\} = \frac{\Delta y \Delta t}{2} u_i^*(T^*_{(i+1)} - T^*_{(i-1)}) \quad (61)$$

$$\int_{t(k)}^{t(k+1)} \int_{y_{(j-\frac{1}{2})}}^{y_{(j+\frac{1}{2})}} \int_{x_{(i-\frac{1}{2})}}^{x_{(i+\frac{1}{2})}} v_j^* \frac{\partial T^*}{\partial y^*} dxdydt = \Delta x \Delta t v_j^*(T^*_{((j+\frac{1}{2})} - T^*_{(j-\frac{1}{2})}) = \Delta x \Delta t v_j^*\{(\frac{T^*_{j+1} - T^*_j}{2}) - (\frac{T^*_j - T^*_{j-1}}{2})\} = \frac{\Delta x \Delta t}{2} v_j^*(T^*_{(j+1)} - T^*_{(j-1)}) \quad (62)$$

$$\int_{t(k)}^{t(k+1)} \int_{y_{(j-\frac{1}{2})}}^{y_{(j+\frac{1}{2})}} \int_{x_{(i-\frac{1}{2})}}^{x_{(i+\frac{1}{2})}} \frac{\partial^2 T^*}{\partial x^{*2})} dxdydt = \Delta y \Delta t \frac{dT^*}{dx^*}\Big|_{i-\frac{1}{2}}^{i+\frac{1}{2}} = \Delta y \Delta t \left(\frac{dT^*}{dx^*}|_{i+\frac{1}{2}} - \frac{dT^*}{dx^*}|_{i-\frac{1}{2}}\right) = \Delta y \Delta t\{(\frac{T^*_{i+1} - T^*_i}{\Delta x}) - (\frac{T^*_i - T^*_{i-1}}{\Delta x})\} = \Delta y \Delta t(\frac{T^*_{i+1} - 2T^*_i + T^*_{i-1}}{\Delta x}) \quad (63)$$

$$\int_{t(k)}^{t(k+1)} \int_{y_{(j-\frac{1}{2})}}^{y_{(j+\frac{1}{2})}} \int_{x_{(i-\frac{1}{2})}}^{x_{(i+\frac{1}{2})}} \frac{\partial^2 T^*}{\partial y^{*2})} dxdydt = \Delta x \Delta t \frac{dT^*}{dy^*}\Big|_{j-\frac{1}{2}}^{j+\frac{1}{2}} = \Delta x \Delta t \left(\frac{dT^*}{dy^*}|_{j+\frac{1}{2}} - \frac{dT^*}{dx^*}|_{j-\frac{1}{2}}\right) = \Delta x \Delta t\{(\frac{T^*_{j+1} - T^*_j}{\Delta y}) - (\frac{T^*_j - T^*_{j-1}}{\Delta y})\} = \Delta x \Delta t(\frac{T^*_{j+1} - 2T^*_j + T^*_{j-1}}{\Delta y}) \quad (64)$$

Hence discretised energy equation is

$$\frac{\Delta x \Delta y}{\Delta T}\{H_{k+1} - H_k\} + 0.5A\rho(C_p)u_i^*(T^*_{(i+1)} - T^*_{(i-1)}) + 0.5B\rho(C_p)v_j^*(v^*_{(j+1)} - T^*_{(j-1)}) = \frac{k}{U_\infty}\{Q(T^*_{i+1} - 2T^*_i + T^*_{i-1}) + R(T^*_{j+1} - 2T^*_j + T^*_{j-1})\} \quad (65)$$

ISSN No:-2456-2165 https://doi.org/10.38124/ijisrt/25jul1701

Where $S = \frac{\Delta x \Delta y}{\Delta T}$, the simplified discretised energy equation is,

$$S(H_{k+1} - H_k) + 0.5A\rho(C_p)u_i(T_{(i+1)} - T_{(i-1)}) + 0.5B\rho(C_p)v_j(T_{(j+1)} - T_{(j-1)}) = \frac{k}{U_\infty}\{Q(T_{i+1} - 2T_i + T_{i-1}) + R(T_{j+1} - 2T_j + T_{j-1})\} \quad (66)$$

The thermal conductivity of NEPCM is calculated according to the Maxwell model as

$$k_{nf} = k_{PCM}\frac{k_p + 2k_{PCM} - 2(k_{PCM} - k_p)\phi}{k_p + 2k_{PCM} + (k_{PCM} - k_p)\phi} \quad (67)$$

Where k_{PCM}, k_p, and k_{nf} are thermal conductivities of pure PCMs, nanoparticles and NEPCMs respectively. The density of nano-fluid ρ_{nf} is calculated as

$$\rho_{nf} = (1 - \phi)\rho_{PCM} + \phi\rho_p \quad (68)$$

Where ρ_{PCM}, and ρ_p are densities of pure and nanoparticles. The heat capacitance of NEPCMs $(\rho c_p)_{nf}$ is defined as

$$(\rho c_p)_{nf} = (1 - \phi)(\rho c_p)_{PCM} + \phi(\rho c_p)_p \quad (69)$$

Where $(\rho c_p)_{PCM}$ is the heat capacitance of the PCM, and $(\rho c_p)_p$ is the heat capacitance of nanoparticles. thermal expansion volume of NEPCMs $(\rho\beta)_{nf}$ is given as

$$(\rho\beta)_{nf} = (1 - \phi)(\rho\beta)_{PCM} + \phi(\rho\beta)_p \quad (70)$$

Where $(\rho\beta)_{PCM}$ and $(\rho\beta)_p$ are thermal expansion volume of pure PCM and nanoparticles respectively. The latent heat of NEPCMs is computed as

$$(\rho L)_{nf} = (1 - \phi)(\rho L)_{PCM} \quad (71)$$

Where $(\rho L)_{PCM}$ is the latent heat of pure PCM. Then the corresponding enthalpy of NEPCM H_{nf} is given as

$$H_{nf} = Cp_{nf}(T - T_r) + f_l L_{nf} \quad (72)$$

IV. RESULTS

➢ *Parameter Estimation*

The numerical simulations depends on the following parameters estimated in Table I.

Table 1 Parameter Estimation (Estimation is Based on Aluminum Oxide)

Parameter	Description	Value Range	Value Used	Value Computed	Units	Source
ρ_p	Density of Al_2O_3	$4 - 4.95$	4.5	–	g/cm^3	[56]
ρ_{PCM}	Density of $NaNO_3$	2.26	–	2.17		[54]
	Density of KNO_3	2.11	–			[55]
ρ_w	Density of Water	0.997	–			[50]
Cp	Heat capacity of Al_2O_3	$0.849 - 0.9$	0.88	–	$J/g \cdot K$	[49]
Cp_{PCM}	Heat capacity of $NaNO_3$	$0.072 - 0.298$	0.129	0.137		[48]
	Heat capacity of KNO_3	0.142	–			[53]
Cp_w	Heat capacity of Water	4.18	–			[50]
β_p	Thermal expansion of Al_2O_3	75×10^{-6}	–	75×10^{-6}	$1/K$	[58]
β_{PCM}	Thermal expansion of $NaNO_3$	83×10^{-6}	–	57.2×10^{-6}		[51]
	Thermal expansion of KNO_3	$30 - 100 \times 10^{-6}$	40×10^{-6}			[52]
β_w	Thermal expansion of Water	207×10^{-6}	–			[50]
k_p	Thermal conductivity of Al_2O_3	237	–	–	$W/m \cdot K$	[60]
k_{PCM}	Thermal conductivity of $NaNO_3$	$0.5 - 0.512$	0.512	0.58		[57]
	Thermal conductivity of KNO_3	0.62	–			[59]
k_w	Thermal conductivity of Water	0.6	–			[50]

ISSN No:-2456-2165 https://doi.org/10.38124/ijisrt/25jul1701

➢ *Numerical Simulations*

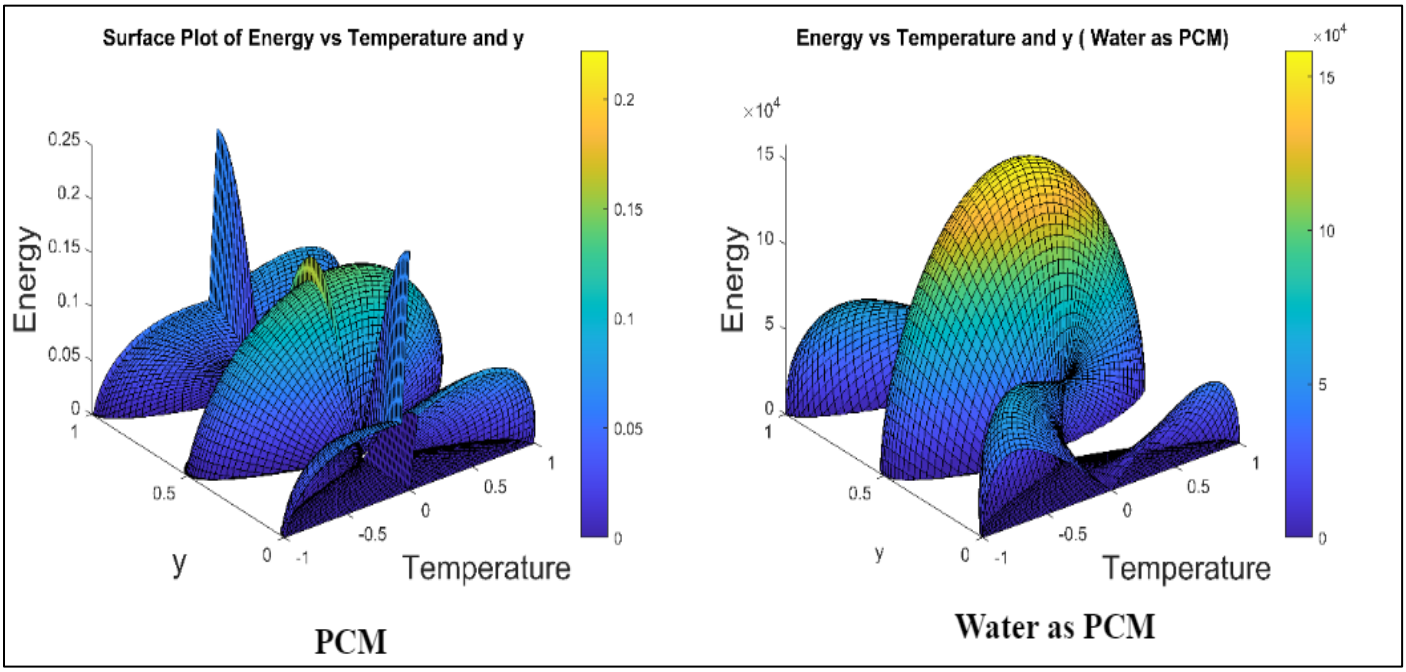

Fig 4 Surface Plot of Energy vs Temperature and y-Axis

Fig 4 presents a 3D surface plot that illustrates the relationship between energy, temperature, and the spatial y-axis in a thermal energy storage system employing nano-enhanced PCMs. The plot visualizes how the introduction of nanoparticles modifies the energy storage characteristics. The x-axis denotes the PCM temperature, which plays a crucial role in phase change dynamics such as melting or solidification. The y-axis represents spatial variation, potentially linked to material layering or different nanoparticle distributions across the domain.

The z-axis (energy) reveals sharp peaks at specific temperature bands, indicating significant latent heat absorption or release associated with phase transitions. These peaks are non-uniform, implying that the presence and concentration of nanoparticles induce localized energy enhancement or suppression. The smooth transition in the colormap from deep blue (low energy) to bright yellow (high energy) enables the identification of thermal hotspots, which are critical for optimizing the charging and discharging cycles of thermal energy storage systems. The figure demonstrates the importance of nanoparticle loading and dispersion in enhancing thermal conductivity, reducing supercooling, and accelerating heat distribution.

The second surface plot represents a similar relationship for a thermal energy system utilizing pure water as the PCM, excluding nanoparticles. In this case, the z-axis energy values are significantly higher in magnitude, as shown by the vertical scale reaching up to 1.6×10^4, a direct result of water's high specific heat capacity (~4180 J/kg·K) compared to common salt-based PCMs or nano-enhanced systems. Unlike the nano-enhanced PCM surface, the energy distribution here is smoother and more symmetric. There are fewer sharp localized peaks, suggesting that pure water stores thermal energy in a more uniformly distributed fashion. The absence of nanoparticle-induced thermal conductivity enhancements means that energy exchange is governed predominantly by water's intrinsic thermophysical properties. This leads to broader thermal gradients and more gradual energy storage, which may be advantageous in systems that require thermal buffering rather than rapid charging/discharging. The color gradient spans from low energy regions (deep blue) to high-energy zones (bright yellow), but the increase in energy appears more continuous and less dependent on spatial variations along the y-axis. This indicates that the system's behavior is more isotropic and homogenous in the absence of nanoparticles.

The comparison between nano-enhanced PCM and water-based PCM shows a clear trade-off between thermal response sharpness and energy capacity. Nano-enhanced PCMs are tailored for high-efficiency, fast response thermal systems, where controlling phase change and thermal gradients is essential. In contrast, water as PCM, with its high specific heat and broader thermal energy profile, suits applications requiring bulk heat storage, passive cooling, or thermal regulation. Both plots reveal the importance of matching PCM material characteristics with system requirements, whether prioritizing energy density, responsiveness, or thermal stability. Based on these observations, Nano-enhanced PCMs are generally better suited for high-performance, compact, and responsive TES applications due to their improved thermal properties, particularly thermal conductivity and phase change efficiency. Water, although abundant and inexpensive, is more useful where bulk energy storage and gradual thermal regulation are sufficient.

ISSN No:-2456-2165 https://doi.org/10.38124/ijisrt/25jul1701

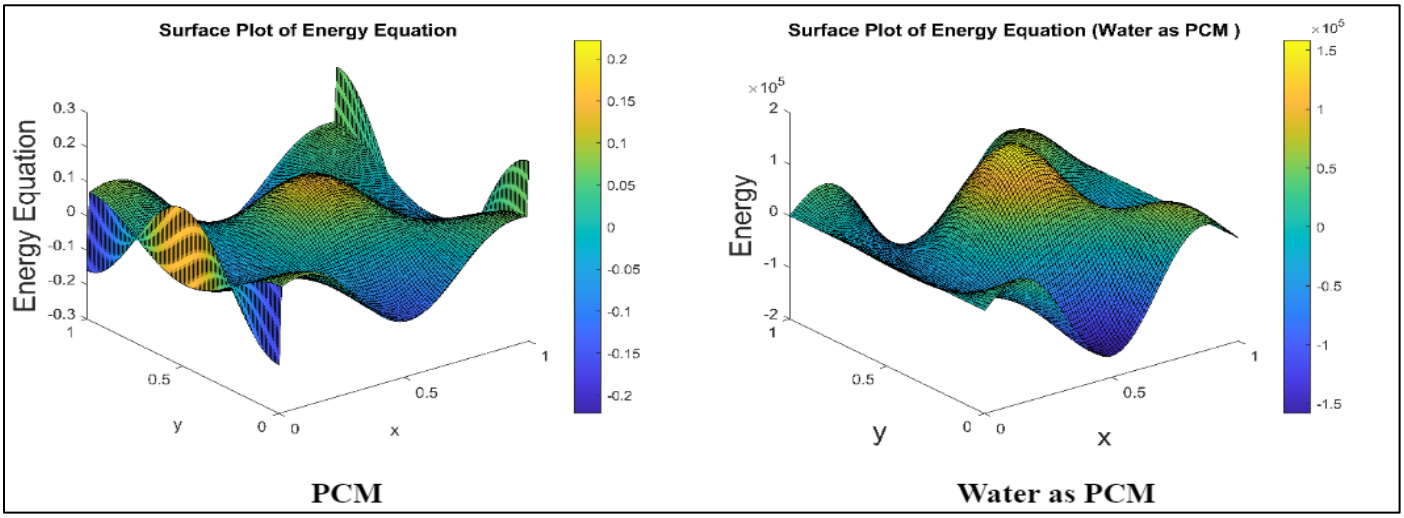

Fig 5 3D Surface Plot of Energy Equation

The left plot in Fig 5 presents a 3D surface visualization of an energy distribution function over spatial coordinates x and y within a nano-enhanced PCM. The surface is characterized by multiple oscillations with both positive and negative values on the z-axis, signifying dynamic energy variation across the domain. Sharp peaks and troughs reflect localized zones of intense energy exchange, corresponding to rapid latent heat absorption or release, which is a direct consequence of the enhanced thermal conductivity and responsiveness introduced by nanoparticles. This pattern suggests high spatial sensitivity, making nano-enhanced PCMs suitable for fast-acting thermal regulation, such as in electronics, concentrated solar power (CSP), or battery systems. The colormap spans a wide dynamic range, from blue (energy deficit) to yellow (energy surplus), indicating the ability of the nano-enhanced PCM system to capture and respond to intricate thermal gradients with efficiency.

The right plot reflects the same energy equation applied to pure water as the Phase Change Material. Unlike the nano-enhanced PCM, the energy distribution in this plot shows a smoother, more symmetric wave pattern, with less abrupt peaks but significantly higher amplitude, as indicated by the z-axis range reaching above 1.5×10^5. This considerable magnitude reflects water's high specific heat capacity (Cp ≈ 4180 J/kg·K), which allows it to store large amounts of sensible heat even in the absence of a phase change within normal temperature ranges. However, since water does not undergo a latent heat transition (melting/solidification) above 0°C, its energy interaction remains continuous rather than discrete. The uniformity across x and y suggests a more homogeneous energy absorption behavior, making water-based systems suitable for passive energy storage, thermal buffering, or building climate moderation, but less optimal for rapid-response thermal management.

The two plots reflect fundamentally different thermal behaviors: Nano-enhanced PCMs demonstrate highly responsive, localized energy fluctuations, making them ideal for systems requiring precise temperature regulation, fast charging/discharging, and latent heat utilization. Water as a PCM, on the other hand, showcases a massive energy storage capacity due to its high specific heat, but lacks the sharp transitions needed for responsive applications. It's best for passive systems and steady-state energy modulation.

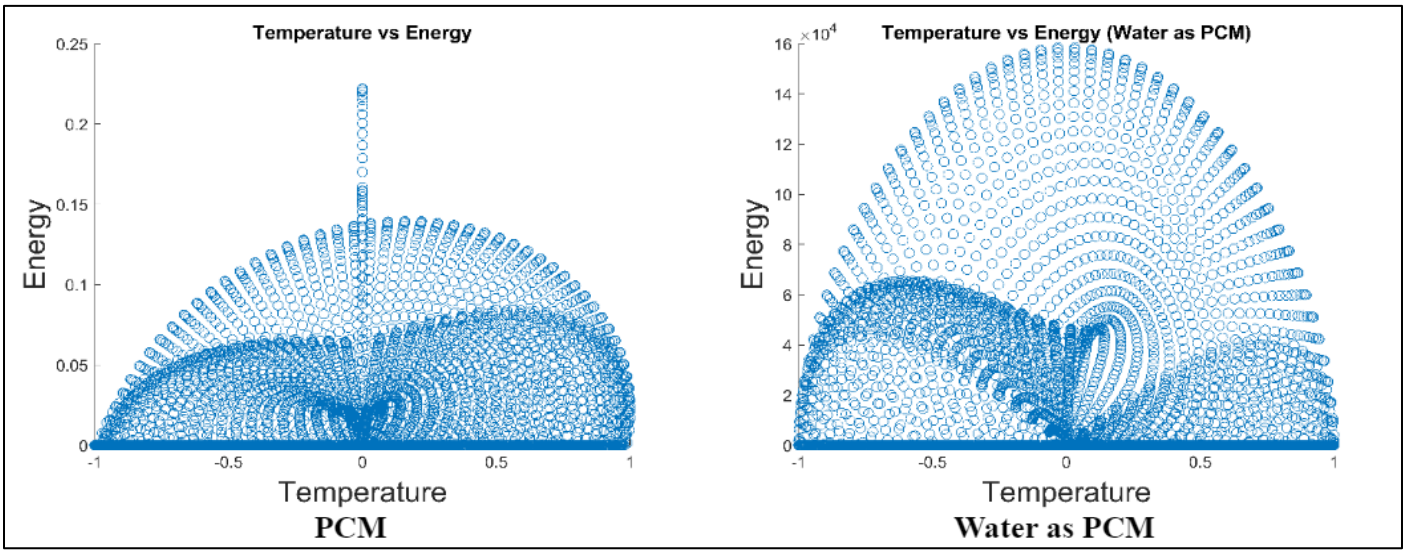

Fig 6 Energy Against Temperature

ISSN No:-2456-2165 https://doi.org/10.38124/ijisrt/25jul1701

Fig 6 (left) presents a scatter plot showing the relationship between temperature and energy for a nano-enhanced Phase Change Material (PCM) under thermal energy storage conditions. The data points form a series of smooth semicircular bands, each indicating a distinct energy behavior over a range of temperatures. These curves are characteristic of cyclical phase transitions, particularly melting and solidification, where latent heat is absorbed or released. The clustering of points around specific temperature values (e.g., near 0°C) signifies phase transition zones, which are indicative of the PCM undergoing thermal transformations. The vertical energy spikes suggest rapid energy absorption during melting, a hallmark of nano-enhanced PCMs optimized for heat transfer. Because only positive energy values are plotted, the figure likely illustrates the charging phase (energy input), rather than cooling or discharging. The overall symmetry and distribution reflect the improved thermal conductivity and responsiveness imparted by the nanoparticles. This behavior is particularly desirable in solar thermal storage, waste heat recovery, and thermal management in electronics, where precise control over phase change timing and energy flow is critical.

The right-side plot illustrates the same Temperature vs Energy relationship for pure water used as a PCM. Visually, it shares the semicircular band structure seen in the nano-enhanced PCM, but with two notable differences: Energy Magnitude: The z-axis (energy) scales up to 1.6×10^4, nearly two orders of magnitude higher than the nano-enhanced PCM. This is due to water's very high specific heat capacity (4.18 J/g·K), which dominates the energy accumulation, even without undergoing a latent phase transition in the temperature range shown. Distribution Spread: The scatter points show denser and more uniform arcs, indicating more continuous, sensible heat-based energy storage rather than sharp transitions seen with latent heat. This reflects water's capacity to gradually absorb heat over a wide range of temperatures, without sharp enthalpic jumps. There are no clustered spikes like those in the nano-enhanced PCM plot, because pure water does not experience a solid–liquid phase change above 0°C in practical applications. Instead, it stores energy linearly and smoothly, suiting it more for thermal buffering, passive cooling, and energy moderation in buildings or slow-response systems.

Nano-enhanced PCM systems offer sharp, well-defined energy-temperature relationships due to latent heat effects, making them ideal for precision TES where phase transitions are leveraged for thermal control. Water as PCM, while incapable of undergoing a latent transition within the observed range, exhibits massive sensible heat storage, rendering it useful for high-capacity, slow-response systems.

V. CONCLUSION

The comparative analysis of nano-enhanced PCMs and water-based PCMs in thermal energy storage reveals critical differences in their thermal behavior and application suitability. The 3D surface plots in Fig. 4 and Fig. 5 show how energy distribution varies with temperature and spatial coordinates. For nano-enhanced PCMs, these figures exhibit sharp, localized peaks corresponding to latent heat absorption and release during phase transitions. These peaks are indicative of highly responsive thermal dynamics resulting from the improved thermal conductivity and heat transfer properties conferred by nanoparticle dispersion. In contrast, water as a PCM displays smooth and symmetric energy surfaces with significantly higher energy magnitudes, reflecting its high specific heat capacity and dominant sensible heat storage mechanism. However, the absence of sharp peaks implies a slower and more uniform thermal response, limiting its effectiveness in systems requiring rapid energy exchange.

Fig. 6 further emphasizes these distinctions by visualizing the relationship between temperature and energy. The nano-enhanced PCM plot reveals clear semicircular bands and clustered spikes at specific temperature zones, consistent with phase change processes. These features enable precise thermal control, making nano-enhanced PCMs ideal for applications such as electronics cooling, solar thermal systems, and waste heat recovery. Conversely, the water PCM plot presents broad, dense energy arcs with no distinct phase transition zones. This highlights its capability for gradual energy absorption and uniform heat distribution, making it suitable for passive thermal management and buffering applications.

From the findings, it is evident that nano-enhanced PCMs are better suited for high-performance, compact, and responsive TES applications, where thermal gradients need to be managed effectively and latent heat can be harnessed to enhance energy efficiency. On the other hand, water-based PCMs are most effective in low-cost, large-scale applications where thermal buffering and storage capacity outweigh the need for responsiveness. The simulations also confirm that enthalpy and temperature are directly correlated, with nanoparticles significantly influencing the energy exchange rate and enhancing thermal uniformity. Although fluid velocity was not explicitly modeled, its role in convective heat transfer is indirectly addressed through the improved conductivity and phase response attributed to nanoparticle inclusion.

The visual and numerical findings support the continued development and optimization of nano-enhanced PCMs for energy-intensive and thermally sensitive applications. Future work should incorporate advanced numerical methods and simulation tools, including multi-physics modeling and machine learning, to predict PCM behavior under dynamic operating conditions more accurately. This will facilitate more precise material design and accelerate experimental validation, ultimately contributing to the broader adoption of TES systems for sustainable energy solutions.

REFERENCES

[1]. N Ahmed, KE Elfeky, Lin Lu, and QW Wang. Thermal performance analysis of thermocline combined sensible-latent heat storage system using cascaded-layered pcm designs for medium temperature applications. *Renewable Energy*, 152:684–697, 2020.

ISSN No:-2456-2165 https://doi.org/10.38124/ijisrt/25jul1701

[2]. BR Baliga and SV Patankar. A new finite-element formulation for convection-diffusion problems. *Numerical Heat Transfer*, 3(4):393–409, 1980.
[3]. Yuri Bazilevs and Thomas JR Hughes. Weak imposition of dirichlet boundary conditions in fluid mechanics. *Computers & fluids*, 36(1):12–26, 2007.
[4]. J Chiew, CS Chin, WD Toh, Z Gao, and J Jia. Thermal state-of-expansion or melting of phase change material based heat sink for underwater battery power system. *Journal of Energy Storage*, 26:100956, 2019.
[5]. Sandra Raquel Leite da Cunha and José Lu1̃3053′fs Barroso de Aguiar. Phase change materials and energy efficiency of buildings: A review of knowledge. *Journal of Energy Storage*, 27:101083, 2020.
[6]. Karem Elsayed Elfeky, Abubakar Gambo Mohammed, and Qiuwang Wang. Cycle cut-off criterion effect on the performance of cascaded, sensible, combined sensible-latent heat storage tank for concentrating solar power plants. *Energy*, 230:120771, 2021.
[7]. Moritz Gosses, Wolfgang Nowak, and Thomas Wöhling. Explicit treatment for dirichlet, neumann and cauchy boundary conditions in pod-based reduction of groundwater models. *Advances in water resources*, 115:160–171, 2018.
[8]. Marcus J Grote and Christoph Kirsch. Dirichlet-to-neumann boundary conditions for multiple scattering problems. *Journal of Computational Physics*, 201(2):630–650, 2004.
[9]. Zhidong Han and Alberto Fina. Thermal conductivity of carbon nanotubes and their polymer nanocomposites: A review. *Progress in polymer science*, 36(7):914–944, 2011.
[10]. Feng Hou, Xinjuan Zhao, Hui Wang, and Qinxi Dong. Microstructure-guided computational model for predicting effective thermal conductivity of cementitious composites filled with phase change particles. *Case Studies in Thermal Engineering*, 38:102339, 2022.
[11]. Amin Ramiani Jafari. Phase change modelling with flexible source-based kinetics for non-equilibrium transitions. *International Journal of Thermal Sciences*, 159:106608, 2021.
[12]. Hussam Jouhara, Alina Żabnieńska-Góra, Navid Khordehgah, Darem Ahmad, and Tom Lipinski. Latent thermal energy storage technologies and applications: A review. *International Journal of Thermofluids*, 5:100039, 2020.
[13]. Cao JX, Yan XH, and Y Xiao. Specific heat of single-walled carbon nanotubes: A lattice dynamics study. *Journal of the Physical Society of Japan*, 72(9):2256–2259, 2003.
[14]. JWJ Kaiser, S Adami, IS Akhatov, and NA Adams. A semi-implicit conservative sharp-interface method for liquid-solid phase transition. *International Journal of Heat and Mass Transfer*, 155:119800, 2020.
[15]. Karunesh Kant, Amritanshu Shukla, Atul Sharma, and Pascal Henry Biwole. Heat transfer studies of photovoltaic panel coupled with phase change material. *Solar Energy*, 140:151–161, 2016.
[16]. Sameer Khare, Mark Dellâ€™Amico, Chris Knight, and Scott McGarry. Selection of materials for high temperature latent heat energy storage. *Solar energy materials and solar cells*, 107:20–27, 2012.
[17]. Rahul Khatri, Rahul Goyal, and Ravi Kumar Sharma. Advances in the developments of solar cooker for sustainable development: A comprehensive review. *Renewable and Sustainable Energy Reviews*, 145:111166, 2021.
[18]. Dai Liu, Long Xin-Feng, Lou Bo, Zhou Si-quan, and Xu Yan. Progress in thermochemical energy storage for concentrated solar power: A review. *International journal of energy research*, 42(15):4546–4561, 2018.
[19]. Maoyuan Liu, Patrick Masset, and Angus Gray-Weale. Solubility of sodium in sodium chloride: a density functional theory molecular dynamics study. *Journal of The Electrochemical Society*, 161(8):E3042, 2014.
[20]. D Lopes, R Agujetas, Hélder Puga, J Teixeira, R Lima, JP Alejo, and C Ferrera. Analysis of finite element and finite volume methods for fluid-structure interaction simulation of blood flow in a real stenosed artery. *International Journal of Mechanical Sciences*, 207:106650, 2021.
[21]. Sidi El Becaye Maiga, Samy Joseph Palm, Cong Tam Nguyen, Gilles Roy, and Nicolas Galanis. Heat transfer enhancement by using nanofluids in forced convection flows. *International journal of heat and fluid flow*, 26(4):530–546, 2005.
[22]. Dnyaneshwar Malwad and Vinod Tungikar. Experimental performance analysis of an improved receiver for scheffler solar concentrator. *SN Applied Sciences*, 2:1–14, 2020.
[23]. Nele Moelans, Bart Blanpain, and Patrick Wollants. An introduction to phase-field modeling of microstructure evolution. *Calphad*, 32(2):268–294, 2008.
[24]. Paul E Ohlsen. Thermal conductivity of sodium chloride within the temperature range 375 k to 637 k. 1956.
[25]. Christos Pagkalos, George Dogkas, Maria K Koukou, John Konstantaras, Kostas Lymperis, and Michail Gr Vrachopoulos. Evaluation of water and paraffin pcm as storage media for use in thermal energy storage applications: A numerical approach. *International Journal of Thermofluids*, 1:100006, 2020.
[26]. SS Parker, NM Abdul-Jabbar, JM Jackson, and M Monreal. Feasibility of volumetric expansion of molten chlorides by conventional pushrod dilatometry. *Journal of Radioanalytical and Nuclear Chemistry*, 331(12):5259–5263, 2022.
[27]. R. Jay Patel, Manish K Rathod, Rajvikram Madurai Elavarasan, and Zafar Said. Influence of longitudinal fin arrangement on the melting and solidification inside the triplex tube latent heat thermal storage system. *Journal of Energy Storage*, 46:103778, 2022.
[28]. Manish K Rathod and Jyotirmay Banerjee. Thermal stability of phase change materials used in latent heat energy storage systems: A review. *Renewable and sustainable energy reviews*, 18:246–258, 2013.
[29]. Zafar Said, Hanin Zeyad, Tasnim I Eisa, and Mamdouh EL Haj Assad. Nano-enhanced pcm for energy storage. In *2019 Advances in Science and Engineering*

ISSN No:-2456-2165 https://doi.org/10.38124/ijisrt/25jul1701

Technology International Conferences (ASET), pages 1–6. IEEE, 2019.

[30]. Atul Sharma, V Veer Tyagi, Carl R Chen, and Dharam Buddhi. Review on thermal energy storage with phase change materials and applications. *Renewable and Sustainable energy reviews*, 13(2):318–345, 2009.

[31]. Paul S Sheeran, Juan D Rojas, Connor Puett, Jordan Hjelmquist, Christopher B Arena, and Paul A Dayton. Contrast-enhanced ultrasound imaging and in vivo circulatory kinetics with low-boiling-point nanoscale phase-change perfluorocarbon agents. *Ultrasound in medicine & biology*, 41(3):814–831, 2015.

[32]. Farooq Sher, Oliver Curnick, and Mohammad Tazli Azizan. Sustainable conversion of renewable energy sources, 2021.

[33]. Asfafaw H Tesfay, Mulu B Kahsay, and Ole J Nydal. Solar cookers with latent heat storage for intensive cooking application. In *ISES Proceedings of Solar World Congress, Daegu, Korea*, volume 8, pages 71–79, 2015.

[34]. Michael Vollmer. Physics of the electromagnetic spectrum. *Electromagnetic technologies in food science*, pages 1–32, 2021.

[35]. Mazlan Abdul Wahid, Seyed Ehsan Hosseini, Hasanen M Hussen, Hussein J Akeiber, Safaa N Saud, and Abdulrahman Th Mohammad. An overview of phase change materials for construction architecture thermal management in hot and dry climate region. *Applied thermal engineering*, 112:1240–1259, 2017.

[36]. Fuzhang Wang, RS Varun Kumar, G Sowmya, Essam Roshdy El-Zahar, BC Prasannakumara, M Ijaz Khan, Sami Ullah Khan, MY Malik, and Wei-Feng Xia. Lsm and dtm-pade approximation for the combined impacts of convective and radiative heat transfer on an inclined porous longitudinal fin. *Case Studies in Thermal Engineering*, 35:101846, 2022.

[37]. Xin Wang, Min Luo, Harshinie Karunarathna, and Dominic E Reeve. An enhanced momentum conservation treatment for fdm simulation of two-phase flows with large density ratio. *Journal of Computational Physics*, 478:111949, 2023.

[38]. M Grae Worster. Instabilities of the liquid and mushy regions during solidification of alloys. *Journal of Fluid Mechanics*, 237:649–669, 1992.

[39]. Shaofei Wu, Ting Yan, Zihan Kuai, and Weiguo Pan. Thermal conductivity enhancement on phase change materials for thermal energy storage: A review. *Energy Storage Materials*, 25:251–295, 2020.

[40]. Lu-Yao Yang, Chang-Ping Feng, Lu Bai, Rui-Ying Bao, Zheng-Ying Liu, Ming-Bo Yang, and Wei Yang. Flexible shape-stabilized phase change materials with passive radiative cooling capability for thermal management. *Chemical Engineering Journal*, 425:131466, 2021.

[41]. Sheng Yang, Xue-Feng Shao, Jia-Hao Luo, Seyedmohsen Baghaei Oskouei, Özgür Bayer, and Li-Wu Fan. A novel cascade latent heat thermal energy storage system consisting of erythritol and paraffin wax for deep recovery of medium-temperature industrial waste heat.

[42]. Zohir Younsi and Hassane Naji. A numerical investigation of melting phase change process via the enthalpy-porosity approach: Application to hydrated salts. *International Communications in Heat and Mass Transfer*, 86:12–24, 2017.

[43]. Malik Sarmad Zahid, Naveed Ahmed, Mumtaz A Qaisrani, Mariam Mahmood, Majid Ali, Adeel Waqas, and Mohsen Assadi. Charging and discharging characterization of a novel combined sensible-latent heat thermal energy storage system by experimental investigations for medium temperature applications. *Journal of Energy Storage*, 55:105612, 2022.

[44]. Mostafa M Zaytoun, Mohaned M El-Bashouty, Medhat M Sorour, and Mohamed A Alnakeeb. Heat transfer characteristics of pcm inside a modified design of shell and tube latent heat thermal energy storage unit. *Case Studies in Thermal Engineering*, 49:103372, 2023.

[45]. Myrto Zeneli, Aris Nikolopoulos, Sotirios Karellas, and Nikolaos Nikolopoulos. Numerical methods for solid-liquid phase-change problems. In *Ultra-high temperature thermal energy storage, transfer and conversion*, pages 165–199. Elsevier, 2021.

[46]. Shuai Zhang, Daili Feng, Lei Shi, Li Wang, Yingai Jin, Limei Tian, Ziyuan Li, Guoyong Wang, Lei Zhao, and Yuying Yan. A review of phase change heat transfer in shape-stabilized phase change materials (ss-pcms) based on porous supports for thermal energy storage. *Renewable and Sustainable Energy Reviews*, 135:110127, 2021.

[47]. Pengbo Zhao, Renkun Dai, Wei Li, Qiuwang Wang, and Min Zeng. Modeling the mushy zone during the melting process under neumann boundary condition using the improved enthalpy-porosity method. *Numerical Heat Transfer, Part A: Applications*, 78(8):423–442, 2020.

[48]. Octav Enea, Prem Paul Singh, Earl M Woolley, Keith G McCurdy, and Loren G Hepler. Heat capacities of aqueous nitric acid, sodium nitrate, and potassium nitrate at 298.15 k: δcpo of ionization of water. *The Journal of Chemical Thermodynamics*, 9(8):731–734, 1977.

[49]. TK Engel. The heat capacities of al2o3, uo2 and puo2 from 300 to 1100 k. *Journal of Nuclear Materials*, 31(2):211–214, 1969.

[50]. William M Haynes. *CRC handbook of chemistry and physics*. CRC press, 2016.

[51]. M Md Ibrahim, V Ramachandran, K Sarangapani, and R Srinivasan. Thermal expansion of sodium nitrate (i). *Journal of Physics and Chemistry of Solids*, 47(5):517–520, 1986.

[52]. Mengting Ji, Laiquan Lv, Jingwen Liu, Yan Rong, and Hao Zhou. Nano3-kno3/eg/al2o3 shape-stable phase change materials for thermal energy storage over a wide temperature range: Sintering temperature study. *Solar Energy*, 258:325–338, 2023.

[53]. M Kawakami, K Suzuki, S Yokoyama, and T Takenaka. Heat capacity measurement of molten nano3-nano2-kno3 by drop calorimetry. In *VII International Conference on Molten Slags Fluxes and Salts, The South African Institute of Mining and Metallurgy*, pages 201–208, 2004.

ISSN No:-2456-2165 https://doi.org/10.38124/ijisrt/25jul1701

[54]. Mark A Kedzierski. Viscosity and density of aluminum oxide nanolubricant. *international journal of refrigeration*, 36(4):1333–1340, 2013.
[55]. Wolfgang Laue, Michael Thiemann, Erich Scheibler, and Karl Wilhelm Wiegand. Nitrates and nitrites. *Ullmann's Encyclopedia of Industrial Chemistry*, 2000.
[56]. Maoyuan Liu, Patrick Masset, and Angus Gray-Weale. Solubility of sodium in sodium chloride: a density functional theory molecular dynamics study. *Journal of The Electrochemical Society*, 161(8):E3042, 2014.
[57]. Ruguang Li, Jiaoqun Zhu, Weibing Zhou, Xiaomin Cheng, and Yuanyuan Li. Thermal properties of sodium nitrate-expanded vermiculite form-stable composite phase change materials. *Materials & design*, 104:190–196, 2016.
[58]. Hsin-Yi Peng, Yi-An Wei, Kao-Chi Lin, Shen-Fu Hsu, Jyh-Chern Chen, Chin-Pao Cheng, and Chan-Shan Yang. Terahertz characterization of functional composite material based on abs mixed with ceramic powder. *Optical Materials Express*, 13(9):2622–2632, 2023.
[59]. Melina Roshandell. *Thermal Conductivity Enhancement of High Temperature Phase Change Materials for Concentrating Solar Power Plant Applications*. PhD thesis, UC Riverside, 2013.
[60]. Ailing Zhang and Yanxiang Li. Thermal conductivity of aluminum alloysâ€"a review. *Materials*, 16(8):2972, 2023.